



# A Mixed Lubrication Model of Liquid/Gas Mechanical Face Seals<sup>©</sup>

BO RUAN

A. W. Chesterton Company  
 Groveland, Massachusetts 01834

and

RICHARD F. SALANT (Member, STLE) and ITZHAK GREEN (Member, STLE)

Georgia Institute of Technology  
 School of Mechanical Engineering  
 Atlanta, Georgia 30332

*A mixed lubrication model for axisymmetric seals, intended as a practical design tool, has been developed. The model considers such physical mechanisms as surface roughness effects on the film lubri-*

*cation, elastic-plastic face contact, face deformation caused by pressure and contact forces, thermal deformation due to viscous and frictional heating, phase change, and temperature and viscosity variations in the film. A numerical scheme that utilizes the influence coefficient method to calculate the face deformations has been developed. This scheme considerably reduces computation time while still maintaining the accuracy of the results. Numerical results obtained through parametric studies show good agreement with available test data.*

Presented at the 52nd Annual Meeting  
 in Kansas City, Missouri  
 May 18-22, 1997

Final manuscript approved February 11, 1997

## NOMENCLATURE

$A_n$  = nominal contact area  
 $b, c, K, n$  = constants  
 $d$  = separation between two surfaces' mean lines  
 $E, \nu$  = Young's modulus and Poisson's ratio  
 $F_e, F_p$  = elastic and plastic contact force  
 $F_{closing}, F_{opening}$  = closing and opening force  
 $F_{contact}$  = contact force  
 $F_{spring}$  = spring force  
 $F_{pressure}$  = fluid pressure force  
 $h$  = nominal film thickness  
 $h_m$  = minimum film thickness  
 $h_{fg}$  = phase change enthalpy  
 $H$  = hardness of the softer material  
 $Ht$  = heat transfer coefficient, normalized with respect to base case  
 $m_g, m_l$  = mass flow rate for gas and liquid  
 $M_{ij}$  = mechanical influence coefficients  
 $p_{atm}$  = atmospheric pressure  
 $p_s$  = sealed pressure  
 $p_{sat}$  = reference saturation pressure  
 $p_i, p_o$  = pressure at ID and OD  
 $q$  = heat generation  
 $q_{friction}, q_{viscous}$  = frictional and viscous heat generation  
 $r_i, r_o, r_b$  = inner, outer, and balance radii  
 $R$  = radius of asperity peaks  
 $R_{gas}$  = gas constant  
 $S_i$  = sealed pressure, atmospheric pressure, spring influence coefficient

$T_b$  = boiling temperature  
 $T_{sat}$  = reference saturation temperature  
 $T_\infty, T_{ref}, T_o$  = reference temperatures  
 $T_{ij}$  = temperature influence coefficients  
 $TH_{ij}$  = thermal influence coefficients  
 $U$  = sliding speed  
 $z$  = asperity height

## Greek Letters

$\alpha$  = thermal expansion coefficient  
 $\gamma$  = surface orientation parameter  
 $\delta$  = change in film thickness due to face deformation  
 $\eta$  = asperity density  
 $\lambda$  = relaxation factor  
 $\mu, \mu_f$  = viscosity, friction coefficient  
 $\mu_o$  = reference viscosity  
 $\rho$  = density  
 $\sigma$  = standard deviation of the surface roughness  
 $\tau$  = shear stress  
 $\phi_r$  = pressure flow factor in radial direction  
 $\phi(z)$  = Gaussian distribution density function of surface height  $z$   
 $\Omega$  = angular velocity  
 $\omega$  = asperity contact interference  
 $\omega_c$  = critical interference

## Subscripts

$i, j$  = Nodes  $i$  and  $j$   
 $1, 2$  = Materials 1 and 2

## KEY WORDS

Rotary Seals, Mechanical Seals, Face Seals

## INTRODUCTION

Mechanical seals often operate with hazardous liquids or gases. Minimizing the leakage is essential in these seal applications. Ideally, to achieve minimum leakage, the two opposing seal faces should be kept as close as possible but still be separated with a thin film so that direct solid contact and severe face damage can be avoided. However, evidence from many industrial applications has shown that low leakage seals very often experience face contact to various degrees and can still function well when properly designed. In such cases the seal operates in the mixed lubrication regime.

In mixed lubrication, the film between the faces is extremely thin, possibly on the order of the surface roughness. The flow field in the film is not only dependent on the face profile, as it is in full film lubrication, but also on the surface roughness as well. The degree of asperity contact is also dependent on both the face profile and the surface roughness. Conversely, the behavior of the flow field and the face contact determine how the seal faces will deform, which dictates the face profile. Therefore, the overall seal performance characteristics, such as leakage, film thickness and temperature increase, are strongly related to the interaction between the film lubrication, the asperity contact, and the deformation processes.

The surface roughness effect on lubrication was studied as early as 1967 by Tzeng and Saibel (1). They used stochastic concepts to study the one-dimensional roughness effects of a slider bearing. This random analysis was further developed soon afterward (2)–(4). Most of these works, however, are limited to one-dimensional roughness. To overcome this weakness, Patir and Cheng (5), (6) developed an average flow model (PC model) by modifying the Reynolds equation with flow factors, which were calculated through numerical simulation based on statistically viable roughness structures. These flow factors take into account the roughness effect on the flow field. Compared with the stochastic approach, the average flow model can be used with general two-dimensional roughnesses and, most importantly, can be applied in the mixed lubrication regime where the roughness effect is most significant.

Later, Elrod (7) and Tripp (8) derived analytical expressions for the flow factors using the method of perturbation expansion. Their work showed good agreement with the average flow model, which provided an analytical base for the flow factor approach. Concurrently, detailed numerical studies were made by Tøndér (9), Teale and Lebeck (10), and Hu and Zheng (11) focusing on the effects of boundary conditions and grid system on obtaining the flow factors through numerical simulation. These studies showed that the average flow model provides a useful tool to study mixed lubrication.

Significant progress has also been made in the study of asperity contact. Abbott and Firestone (12) introduced the simple plastic contact model between a rough surface and a flat face. This model was improved by Pullen and Williamson (13) to consider volume conservation of the asperities during

plastic deformation. Since the plastic contact model assumes that yielding occurs during asperity contact, it may be more suited for heavily loaded contacts. For lightly loaded contacts, the elastic contact model developed by Greenwood and Williamson (14) is more appropriate. This model combines Hertzian contact theory with a statistical treatment of the surface roughness. The elastic contact model that was originally developed for the contact of nominally parallel surfaces was extended by Greenwood and Tripp (15) to include the contact of a curved surface against a flat surface. Neither of the latter two models, however, can be applied under moderate loading conditions, where both plastic and elastic deformation occur. For this case, Chang et al. (16) developed a more general elastic-plastic contact model by combining Greenwood and Williamson's elastic contact model with the plastic contact model.

Given the considerable progress in understanding the thin film lubrication between rough surfaces and asperity contact behavior, mathematical models of contacting seals have been developed. Lebeck (17) introduced a mixed friction model to analyze a hydrostatic mechanical seal. This model considers load sharing between the fluid pressure and contact load. The pressure is determined by the average flow model while the contact load is computed based on the plastic contact model. Later, the model was extended to the two-phase situation by Lebeck (18). In his models, asperity contact-caused deformation is not considered. Zhu et al. (19), (20) studied the dynamic behavior of piston skirts in mixed lubrication and found that the deformation due to the asperity contact between the piston skirts and the cylinder wall are dominant factors in determining the piston motion. Yamaguchi and Matsuoka (21) introduced a mixed lubrication model that is based on a combination of the average flow model and the elastic contact model. The model considers the effects of EHL, and cavitation at the contact area. However, face deformation was not included in the analysis, which was only suitable for two parallel face conditions. More recently, a similar model based on the elastic-plastic contact model and average flow was developed by Etsion and Front (22). Their study was concerned with hydrostatic seals in the static condition with parallel faces. Mechanical and thermal deformations were not considered in the analysis.

Although many advancements have been made in understanding the mixed lubrication process and developing mathematical models, a comprehensive and practical seal model that can efficiently predict seal performance is still needed. The lack of a practical model to predict the effects of various parameters, such as material, geometries, loading, and surface finish on the leakage rate, face temperature and other characteristics, necessitates the use of trial and error methods for seal designs. This is very time consuming and expensive since extensive laboratory tests are necessary.

The purpose of this study is to present a practical seal model that considers the coupled effects between asperity contact, film lubrication, and face deformation while allowing timely predictions of seal performance under a wide range of parameters (23). The model is intended to be used as a design tool to help optimize seal designs, save design time and give guidance to experimental testing.

## PHYSICAL MODEL

Figure 1 shows a typical pressurized seal configuration. Its operation involves three major physical processes, i.e., the film lubrication process, asperity contact, and the thermal/mechanical deformation of the seal faces. During seal operation, the seal faces are subject to pressure and asperity contact forces, which cause mechanical face deformation. In addition, viscous heat due to fluid shearing and frictional heat generated at the contacting regions cause face thermal deformation. The mechanical and thermal deformations change the face profile which, in turn, determines the pressure distribution in the film and the degree of asperity contact. When excessive heat generation is coupled with a significant pressure drop across the seal faces, the liquid film in the seal gap could vaporize over part of the seal faces, causing a two-phase seal operating situation. Such a change could lead to quite a different performance from its liquid counterpart. Clearly, an accurate prediction of seal performance must take into account the interaction between the film lubrication, solid-to-solid contact, and mechanical/thermal effects.

To develop an efficient seal model, a number of physical assumptions are made in this study as follows:

1. The seal is axisymmetric. Strictly speaking, seals cannot be perfectly axisymmetric during operation, since face asymmetries may develop due to misalignment and non-uniform support of the seal faces. However, as long as the seal is geometrically axisymmetric, the nonaxisymmetric effects can be neglected as a first approximation in the design process. Therefore, the hydrodynamic pressure caused by nonaxisymmetric face features are not considered and only the hydrostatic pressure is assumed to be present in the film.
2. The seal is stable and operates at steady-state about equilibrium.
3. The face deformation under thermal and mechanical effects is small, so that the deformation can be approximated as a linear function of the thermal and mechanical loads. This assumption is justified by the fact that seal face deflection is commonly on the order of micrometers, which is significantly smaller than the face dimensions. In addition, the temperature change is assumed to be linearly dependent on the thermal load.

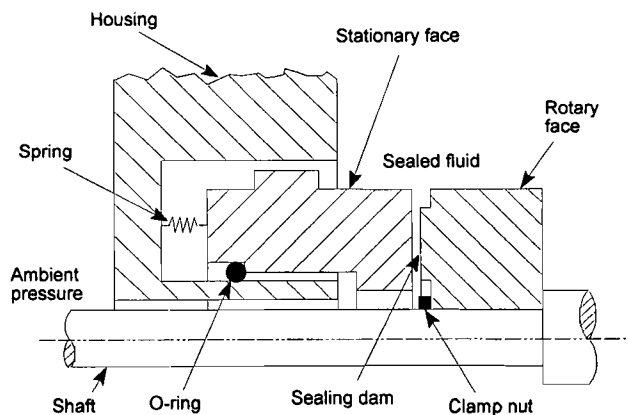


Fig. 1—Schematic of a mechanical seal.

4. Since the film is thin (and opposing faces are close to each other), it is assumed that there is no temperature change across the film, and the film and face temperatures are the same. However, the face temperature does vary in the radial direction, and liquid viscosity, which is strongly dependent on the temperature, varies across the face. In the case of a gas seal, the gas is treated as an ideal gas. This assumption greatly simplifies the analysis; otherwise, exact thermodynamic data must be used for a more precise analysis.
5. The heat convection in the fluid film and the heat of vaporization in the case of a two-phase situation are negligible compared to the heat conducted into the seal faces. For low leakage seals, the amount of heat needed for vaporization, and the convection in the fluid film in general, is insignificant with respect to the total heat generation, which is essentially all conducted into the seal faces.
6. In the two-phase seal analysis, the boiling or phase change takes place at a discrete radial interface, which must be determined. In actuality, boiling occurs over a range of radii.

The above assumptions may appear somewhat restrictive, and some may have to be examined by a more rigorous analysis. However, as a first approximation in the design process, these assumptions simplify the problem and allow an analysis to be carried out as outlined below.

## BASIC EQUATIONS

### Force Balance

During equilibrium operation, the net axial force on the floating seal face must be zero, i.e., the opening force must be equal to the closing force in magnitude but opposite in direction:

$$F_{closing} = F_{opening} \quad [1]$$

The closing force is produced by the sealed pressure and the spring force shown in Fig. 2 and is given by

$$F_{closing} = \pi[(r_o^2 - r_b^2) p_s + (r_b^2 - r_i^2) p_{atm}] + F_{spring} \quad [2]$$

where  $r_o$ ,  $r_i$ ,  $r_b$  are the seal inner, outer, and balance radii, respectively. For a given seal design and geometry, the closing force is a constant and is easy to determine. The opening force consists of the pressure force in the film and the contact force due to asperity contact:

$$F_{opening} = F_{pressure} + F_{contact} \quad [3]$$

Computation of this force requires the coupled analyses of the film lubrication, asperity contact, and face deformation. These analyses are discussed below.

### Film Lubrication

Patir and Cheng (5) proposed an average flow model that includes the effects of the surface roughness on the pressure-

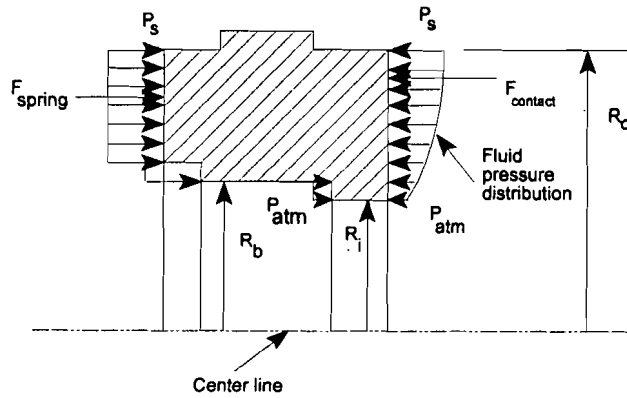


Fig. 2—Equilibrium operation of a mechanical seal.

induced flow. According to this model, the mass flow rate takes the form

$$m_l = -\varphi_r \frac{\pi r p h^3}{6\mu} \frac{dp}{dr} \quad [4]$$

$\varphi_r$  is the pressure flow factor determined through numerical flow simulation of surfaces with multiple asperities. According to Patir and Cheng (5),  $\varphi_r$  can be curve fitted as

$$\varphi_r = 1 - ce^{b(h/\sigma)} \quad \text{for } \gamma \leq 1 \quad [5]$$

or

$$\varphi_r = 1 + c(h/\sigma)^{-b} \quad \text{for } \gamma > 1 \quad [6]$$

where  $c$  and  $b$  are numerical constants, and both  $\sigma$  and  $\gamma$  are roughness parameters.  $\sigma$  is the composite standard deviation of the roughness heights

$$\sigma = (\sigma_1^2 + \sigma_2^2)^{1/2} \quad [7]$$

and  $\gamma$  characterizes the directional property of the roughness. The parameter  $\gamma$  can be visualized as the length-to-width ratio of a representative asperity. For isotropic roughness,  $\gamma$  is equal to 1.

As shown by Patir and Cheng (5), when  $h/\sigma > 3$ ,  $\varphi_r$  approaches unity and the effect of the surface roughness becomes negligible. When  $h/\sigma < 3$ , asperity contact takes place and roughness effect is significant and must be considered.

When the average flow model is combined with the Reynolds equation, a modified Reynolds equation is obtained. For an axisymmetric liquid seal, the appropriate form is

$$\frac{1}{r} \frac{d}{dr} \left( \frac{\varphi_r r p h^3}{12\mu} \frac{dp}{dr} \right) = 0 \quad [8]$$

while for a gas seal

$$\frac{1}{r} \frac{d}{dr} \left( \frac{\varphi_r r p h^3}{12\mu R_{gas} T} \frac{dp}{dr} \right) = 0 \quad [9]$$

Once the pressure distribution is determined, the pressure force can be found by integrating across the seal face:

$$F_{pressure} = 2\pi \int p r dr \quad [10]$$

### Asperity Contact

When two rough surfaces are brought into contact, the contact first takes place at the highest asperity tips. Since the load concentrates at these small contact areas, the stress is high, causing the asperity to deform plastically. As the separation is reduced, more asperities come into contact and the contact load is spread over a larger area. Eventually, an equilibrium separation is reached when the closing force is balanced by the contact force and the pressure force. Some of the asperities have deformed plastically, while the rest of the contacting asperities have deformed elastically.

In the work of Chang et al. (16), the contact between two rough surfaces is represented by a contact between an equivalent rough surface with a smooth surface. The rough surface is modeled by a collection of spherical caps all having a radius of curvature  $R$ , with a certain statistical distribution of their heights.

Given the topography of the contacting surfaces, it was shown by Chang et al. (16) that the contact load of each individual asperity depends only on the interference, defined as

$$\omega = z - d \quad [11]$$

where  $z$  is the asperity height and  $d$  is the separation between the two surfaces. Chang et al. (16) also showed that asperities begin to yield when  $\omega$  reaches the critical interference

$$\omega_c = \left( \frac{\pi KH}{2E} \right)^2 R \quad [12]$$

where

$$\frac{1}{E} = \frac{1 - \nu_1^2}{E_1} + \frac{1 - \nu_2^2}{E_2} \quad [13]$$

and  $E_1, E_2, \nu_1, \nu_2$  are Young's moduli and Poisson's ratios of the contacting surfaces, respectively.  $H$  is the hardness of the softer material and  $K$  is a numerical constant ( $\sim 0.6$ ). Therefore, when  $\omega < \omega_c$ , the contact is elastic. When  $\omega \geq \omega_c$ , the contact is plastic.

By modifying the analysis of Greenwood and Williamson (14), Chang et al. (16) obtained the elastic contact force

$$F_e = \frac{4}{3} \eta A_n E R^{1/2} \int_d^{d+\omega_c} (z - d)^{3/2} \varphi(z) dz \quad [14]$$

where  $\eta$  is the asperity density and  $\varphi(z)$  is the statistical distribution function of the surface height. Based on the volume conservation condition, they also derived the plastic contact force given by

$$F_p = K \pi \eta A_n H R \int_{d+\omega_d}^{\infty} [2(z - d) - \omega_c] \varphi(z) dz \quad [15]$$

Hence, the total contact force is the sum of the contributions of the elastically and plastically deformed asperities, i.e.,

$$F_{contact} = F_e + F_p \quad [16]$$

### Deformation and Temperature

The film thickness distribution is directly influenced by the face deformation. The face deformation consists of thermal and mechanical deformations. The thermal deformation is caused by viscous and frictional heating; the mechanical deformation is caused by fluid pressure and asperity contact forces. The deformations can be calculated by a finite element structural analysis. This method, however, requires a large amount of computing time because these deformation calculations must be repeated many times in each iteration due to the coupling between the lubrication, contact, and deformation processes. To reach an equilibrium solution, there will likely be hundreds of iterations during the entire computation process. For such an analysis to be an efficient design aid, it is important to reduce the computational expense. One alternative is to use the influence coefficient method, which is based on the assumption that the deformation is linearly dependent upon the external loadings. Specifically, the nodal film thickness can be written as

$$h_i = h_m + \delta_i \quad [17]$$

where  $\delta_i$  is determined through the influence coefficient method

$$\delta_i = \sum_{j=1}^n (M_{ij}F_j + TH_{ij}q_j) + S_i \quad [18]$$

$M_{ij}$  and  $TH_{ij}$  are the influence coefficients representing the face deformation at Node  $i$  due to unit mechanical and thermal loads, respectively, at Node  $j$ .  $F_j$  and  $q_j$  represent the actual mechanical and thermal loads, respectively.  $S_i$  is the influence coefficient representing the face deformation at Node  $i$  due to the combined effects of the sealed pressure, atmospheric pressure and the spring force. The influence coefficients can be calculated off line with a finite element analysis, and will be treated as input data to the main program. They are used repeatedly during each iteration. In such a way, a significant amount of computing time is saved without much sacrifice in the accuracy of the results.

Similarly, since the temperature change on the seal faces is linearly related to the heat flux, the nodal temperature change can also be computed via the influence coefficient method

$$\delta T_i = \sum_{j=1}^n T_{ij}q_j \quad [19]$$

where  $T_{ij}$  is the temperature influence coefficient representing the temperature change at Node  $i$  due to a unit heat flux at Node  $j$ . The actual seal face temperature is given by

$$T_i = T_{ref} + \delta T_i \quad [20]$$

where  $T_{ref}$  is the reference temperature, commonly chosen to be the fluid operating temperature in the seal chamber.

### Heat Generation

The heat generation consists of the viscous and frictional heat generation, i.e.,

$$q = q_{viscous} + q_{friction} \quad [21]$$

Given the angular velocity of the rotating face  $\Omega$ , the viscous heat generation can be determined by

$$q_{viscous} = \int_A \tau U dA = \int_A \mu \frac{U^2}{h} dA = \int_A \mu \frac{r^2 \Omega^2}{h} dA \quad [22]$$

It is important to note that the fluid liquid viscosity can be very sensitive to the temperature variations, especially for synthetic oils. In this analysis, a power law relation is used to represent the viscosity-temperature relationship of the liquid film, which is expressed as

$$\mu = \mu_0 \left( \frac{T_0}{T} \right)^n \quad [23]$$

where  $\mu_0$  is the nominal viscosity at the nominal temperature  $T_0$ , and  $n$  is a constant to be determined from empirical viscosity-temperature data.

The frictional heat generation is caused by the solid friction between the contacting asperities and is given by

$$q_{friction} = \mu_f F_{contact} U = \mu_f F_{contact} r \Omega \quad [24]$$

where  $\mu_f$  is the friction coefficient. The friction coefficient depends on the face material, surface finish, fluid properties, operating conditions, and environmental conditions.  $\mu_f$  usually falls in the range of 0.03 to 0.15.

### METHOD OF SOLUTION

The determination of the equilibrium operation of a contacting seal requires numerical iterations as illustrated in the flowchart shown in Fig. 3. Here, the key quantities are the film thickness distribution  $h_i$  and face temperature distribution  $T_i$ , where  $i$  denotes a nodal point at the sealing dam. Once these two variables converge, so do the others.

The computation starts with the initial input, including the influence coefficients, seal geometry, material properties, surface topography, and operating conditions. Then, an estimation of minimum film thickness, face profile, and face temperature is made. This is followed by the first iteration loop, where the contact force (Eq. [16]), pressure distribution (Eq. [8] or [9]), viscous and frictional heat (Eqs. [22] and [24]) are calculated. Then, the film thickness is computed by the influence coefficient method (Eqs. [17]–[20]). The computed film thickness distribution is compared with the results from the last iteration. If the film thickness does not converge, then it is modified as

$$h^{(i+1)} = \lambda h^{(i)} + (1 - \lambda) h^{(i-1)} \quad [25]$$

where  $h^{(i)}$  and  $h^{(i-1)}$  are the film thickness in the current and previous iteration, respectively, and  $\lambda$  is the relaxation

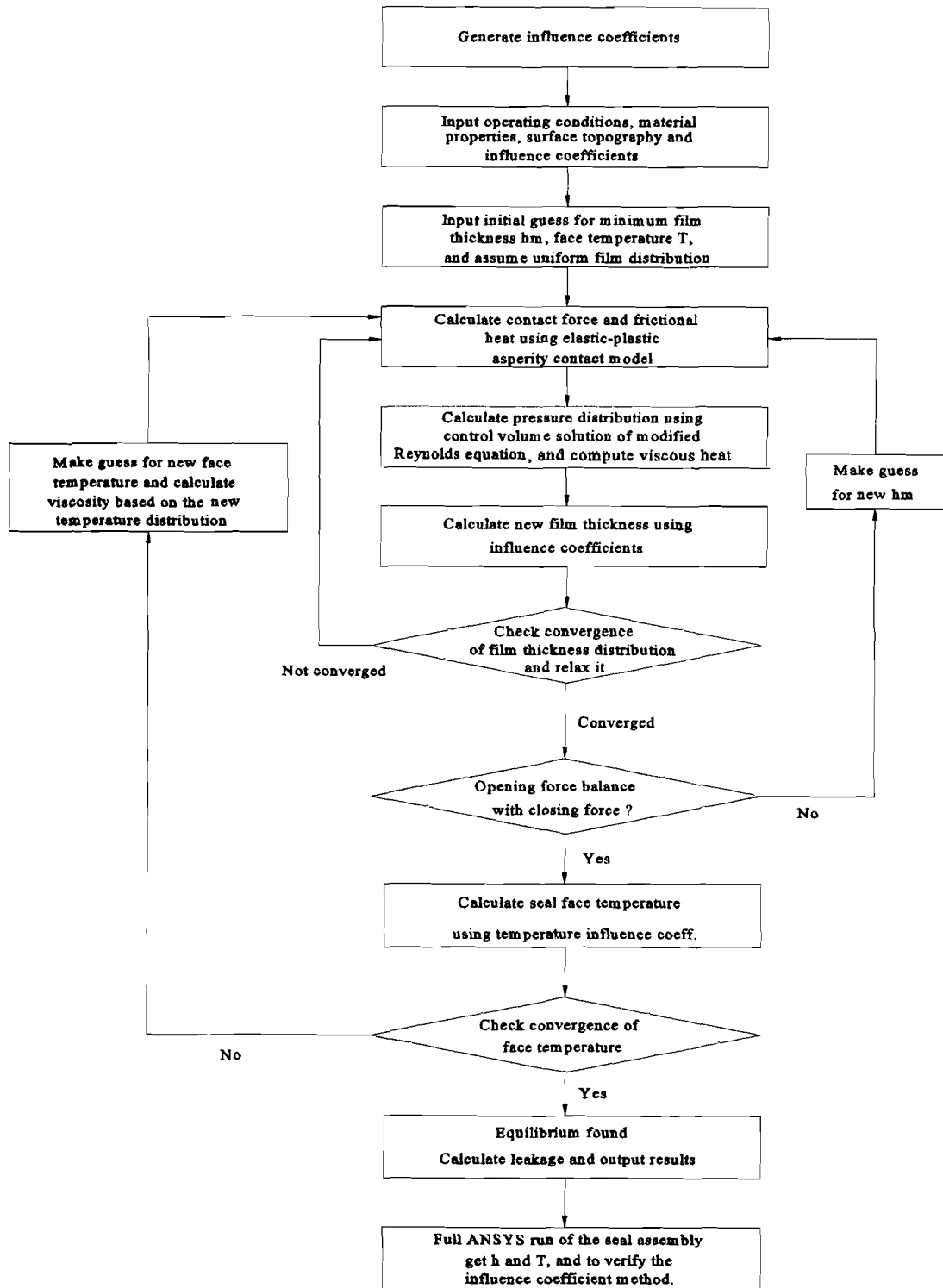


Fig. 3—Flowchart to find equilibrium seal operation.

factor. Values of  $\lambda$  of 0.3 or less are required in order to achieve convergence. When the film thickness converges, the opening force is compared with the closing force. If the forces are not balanced, the minimum film thickness is revised according to

$$h_m^{(i+1)} = \exp \left[ \frac{\Delta f^{(i-1)} \ln h_m^{(i)} - \Delta f^{(i)} \ln h_m^{(i-1)}}{\Delta f^{(i-1)} - \Delta f^{(i)}} \right] \quad [26]$$

where  $\Delta f^{(i)}$  and  $\Delta f^{(i-1)}$  are the differences between the opening force and the closing force at the current and pre-

vious iterations. This interpolation/extrapolation scheme prevents the minimum film thickness from becoming negative. Then, the previous calculations are repeated until the force balance is achieved. As stated above, an estimate of the initial minimum film thickness is made for the first iteration,  $h_m^{(1)}$ . For the second iteration,  $h_m^{(2)}$  is arbitrarily chosen to equal  $0.8 h_m^{(1)}$ . Only then can Eq. [26] be used for the third iteration and beyond.

After the force equilibrium is found, the convergence of face temperature is checked. Only when the temperature has

converged, the steady equilibrium seal operation is found. Otherwise, the face temperature is modified by the bisection method:

$$T^{(i+1)} = \frac{T^{(i)} + T^{(i-1)}}{2} \quad [27]$$

where  $T^{(i)}$  and  $T^{(i-1)}$  are the temperature at the current and the previous iterations, respectively. With the updated temperature, viscosity is recalculated and the iteration process is repeated as described above.

In the case of a two-phase seal, the above procedure requires some modification in the solution of the Reynolds equation for the pressure distribution. The appropriate Reynolds equation is solved separately in the liquid and gas regions, and the mass flow rates at the liquid-vapor interface are matched. Since the location of the liquid-vapor interface,  $r_b$ , is unknown a priori, an iterative procedure is performed as follows:

1. Make an initial estimation of the boiling radius  $r_b$ .
2. Calculate the boiling pressure  $p_b$  using Clapeyron's equation:

$$\frac{p_b}{p_{sat}} = \exp\left[-\frac{h_{fg}}{R_{gas}}\left(\frac{1}{T_b} - \frac{1}{T_{sat}}\right)\right] \quad [28]$$

where  $p_{sat}$  and  $T_{sat}$  are the reference saturation pressure and corresponding temperature, respectively,  $T_b$  is the fluid temperature at the boiling point, and  $h_{fg}$  is the latent heat for phase change.

3. Solve for the pressure distributions and mass flow rates in both the liquid and vapor regions.
4. Compare the mass flow rates in the two regions. If they match, then a solution is obtained. Otherwise, a revised boiling radius is computed via the bisection method.
5. Repeat Steps 2, 3, and 4 until the mass flow rates match.

**RESULTS**

To determine how well the model predicts seal performance, three typical seal cases, namely a gas seal, a liquid seal, and a two-phase seal, were analyzed and the results were compared with test data.

**Gas Seal**

The sealed gas is propane. Figure 4 shows the film thickness distribution under the nominal operating condition. Two curves are presented in the figure. One curve corresponds to the film thickness distribution calculated using the influence coefficients and the other corresponds to the results using a complete finite element analysis. These two curves coincide, indicating the influence coefficient method is successful. It is also seen that the film thickness is quite uniform across the entire seal face with a maximum variation of less than one-tenth of a micron. Experimental observations, based on face wear measurements, reveal that the face is indeed quite even, suggesting a uniform surface profile during seal operation.

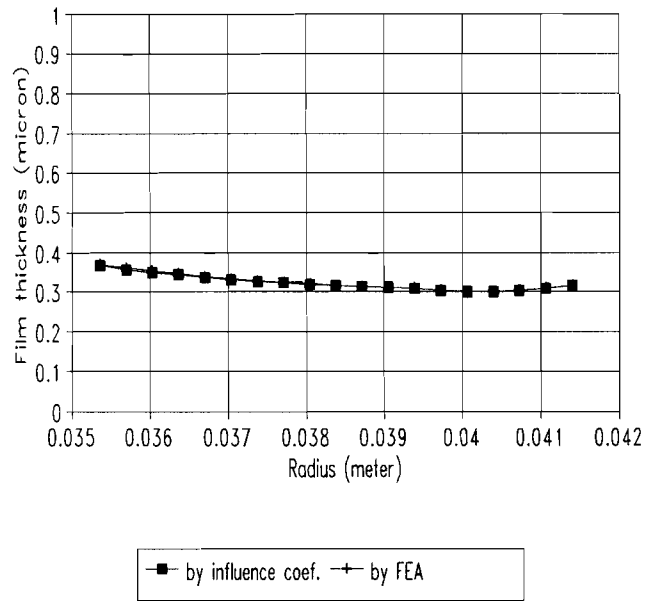


Fig. 4—Film thickness distribution, gas seal.

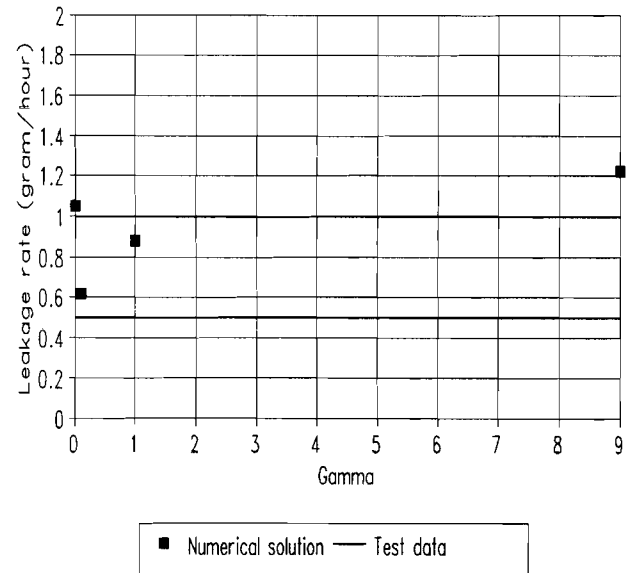


Fig. 5—Effect of  $\gamma$  on leakage rate, gas seal.

The roughness effects on the flow field are illustrated in Fig. 5. The roughness orientation significantly changes the leakage rate as shown in the figure. Four representative roughness orientations were studied: isotropic roughness represented by  $\gamma = 1$ , tangentially oriented roughness ( $\gamma = 1/9$ ), radially oriented roughness ( $\gamma = 9$ ), and ideally smooth surfaces represented by  $\gamma = 0$ . The numerical data shows that as  $\gamma$  increases, the leakage rate generally increases. Physically, this is expected since tangential roughness ( $\gamma = 1/9$ ) radially produces more flow resistance and helps reduce the leakage, while radial roughness ( $\gamma = 9$ ) offers the least resistance to radial flow and leakage. It is interesting to note that the leakage rate for a smooth surface is larger than that for an isotropic surface and less than that for a radial roughness. The test measurements for the leakage rate are in the range of 0.5 to 1.0 gram/hour and are depicted by two solid

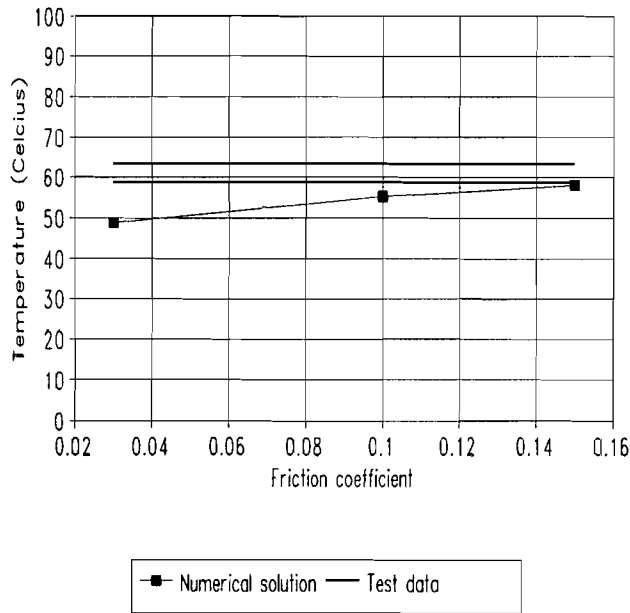


Fig. 6—Friction effect on face temperature, gas seal.

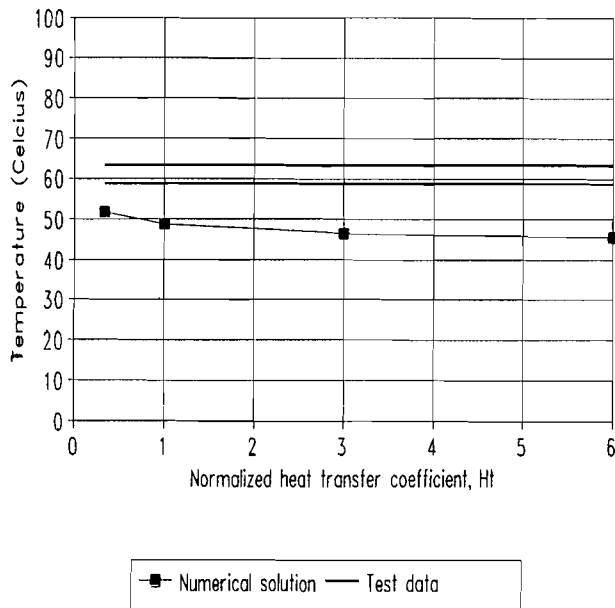


Fig. 7—Convective heat transfer effect on face temperature, gas seal.

lines that represent the bounding values. Except for the  $\gamma = 9$  case, all the computed leakage rates fall within the error brackets of the test results.

The friction coefficient at the contact asperities significantly affects the frictional heat and, ultimately, the face temperature and thermal deformation. That coefficient varies depending on the face materials, fluid, operating conditions, and environmental conditions and is difficult to determine. Data from previous experiments (24) suggest that typical values range from 0.03 to 0.15. In the current simulation, these values were used to study their effects on the face temperature as shown in Fig. 6. The two solid lines bracket the experimental measurements of the face temperatures and represent the bounding values. As the friction coefficient increases, the computed face temperature noticeably increases. At  $\mu_f = 0.15$ , the computed temperature matches the test

data, suggesting that the friction coefficient for the gas seal could be as high as 0.15.

The heat transfer coefficient values are important parameters in the seal analysis since the temperature distribution and thermal deformation are primarily determined by the convective heat transfer in the seal chamber. However, the convective heat transfer involves turbulent flow, a complex physical phenomena that is an ongoing research topic. At the present time, choosing the appropriate convection coefficients relies on engineering judgement, and a degree of uncertainty is involved. In this seal analysis, the convection boundary conditions and the coefficient values were all based on empirical data. Figure 7 shows how the convective heat transfer coefficient values (normalized) affect the seal face temperatures. As expected, the temperature decreases as the heat transfer rate increases. However, the temperature decrease is only 5° to 6°C while the convective heat transfer coefficients have changed by an order of magnitude. This indicates that the temperature is relatively insensitive to the convective heat transfer coefficient. This is because the rate of heat generation in the gas seal is very low and, therefore, changes in the heat removal rate result in little decrease in temperature. The fact that the face temperature is relatively low and the faces are close to parallel, due to small thermal deformation, does show that the heat generation rate is low. However, the situation is different for the liquid seal, as is discussed below.

### Liquid Seal

The sealed liquid is a synthetic oil with a viscosity of  $1.2 \times 10^{-2}$  Pa·s at 40°C,  $2.98 \times 10^{-3}$  Pa·s at 100°C and  $8.9 \times 10^{-4}$  Pa·s at 205°C. The film thickness distribution is shown in Fig. 8. The face exhibits positive coning with a minimum film thickness of approximately 0.3 microns. Possible asperity contact is expected near the ID, and roughness effects could be significant as well. The positive coning was largely caused by the thermal deformation. Compared to the gas case, the liquid viscosity is about two orders of magnitude higher than

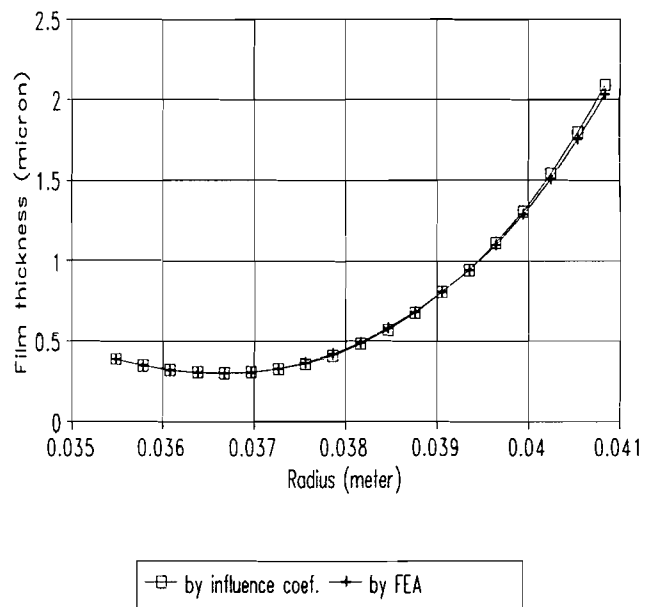


Fig. 8—Film thickness distribution, liquid seal.

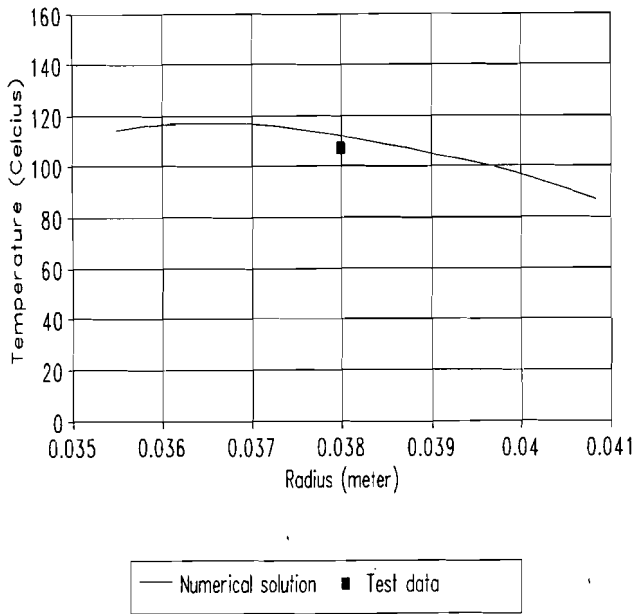


Fig. 9—Face temperature distribution, liquid seal.

the gas (propane) viscosity. The viscous heating is much higher and, thus, causes large positive thermal coning. Even with negative pressure coning, the net coning is still positive. This is unlike the gas seal case, in which the negative pressure coning almost cancels out the positive thermal coning, resulting in negligible coning and a uniform film profile (Fig. 4). The above suggests that thermal heating is particularly important in the liquid seal operation. Figure 8 also shows that the film thickness distribution resulting from the finite element analysis matches very well with the results based on the influence coefficient method.

Figure 9 displays the face temperature variation. The temperature is higher (~118°C) at the ID and lower (~86°C) at the OD since more heat is generated at the ID as seen from the above film thickness distribution. The comparison between the predicted average temperature (~107°C) and the test measurement (~106°C) is very good.

The effect of roughness orientation on the leakage rate is shown in Fig. 10, which exhibits a similar trend as the gas seal. The tangential roughness retards leakage while radial roughness enhances the flow. Since gamma could not be controlled in the test, a single test value of the leakage rate is shown in the figure as a solid line. In comparison with the test data, the numerical prediction underestimates the leakage rate by a factor of two. This could be attributed to the uncertainty in the convective heat transfer coefficient values that were used in the calculations. The thermal deformation is strongly dependent on the convection coefficients and, hence, could significantly affect the leakage rate. Despite the uncertainties in the thermal conditions and the fact that the predicted leakage rate differs from the test data by a factor of two, the obtained result is still considered to be reasonably accurate within the context of the present state of the art of seal performance prediction.

Figure 11 shows that the friction coefficient has little effect on the face temperature. This indicates that there is negligible asperity contact during the seal operation. In fact, the contact load in this case is only about five percent of the total

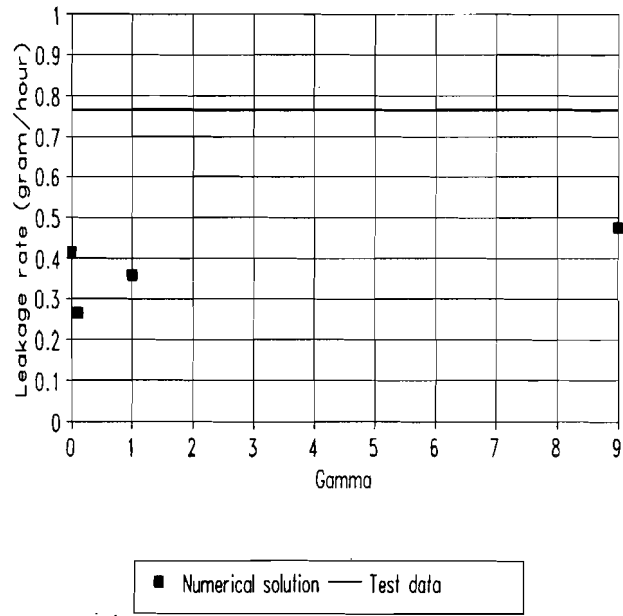


Fig. 10—Effect of  $\gamma$  on leakage rate, liquid seal.

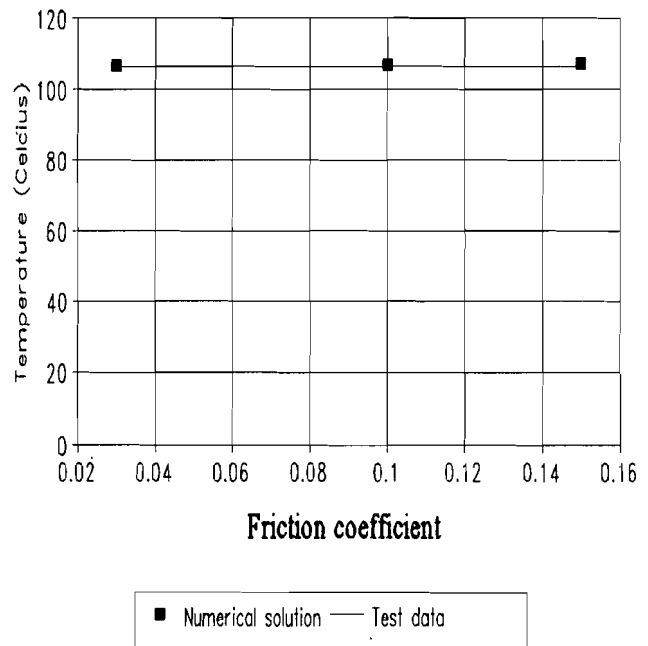


Fig. 11—Friction effect on face temperature, liquid seal.

load support. A majority of the heat generation is caused by the viscous shearing. The predicted temperature matches very well with the test measurement. As in the previous figure, a single test value is shown as a solid line.

Figure 12 shows the normalized heat transfer coefficient effect on the face temperature. Unlike the result obtained for the gas seal, the temperature decreases considerably as the heat transfer increases. The total temperature reduction is approximately 50°C when the convective heat transfer coefficient values have increased by an order of magnitude. Compared with the gas seal case, the temperature is extremely sensitive to the convective heat transfer coefficient under the same operating conditions as in the gas seal, i.e., same frictional coefficient and surface roughness. Such a result indicates that the thermal heating, which is primarily

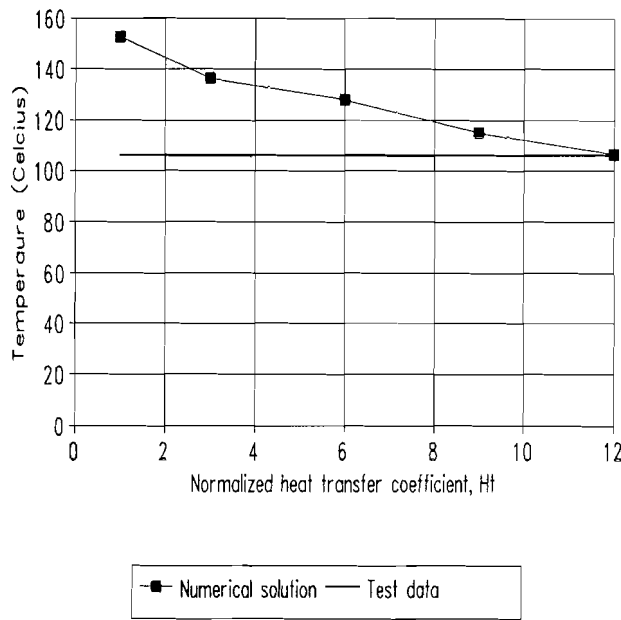


Fig. 12—Convective heat transfer effect on face temperature, liquid seal.

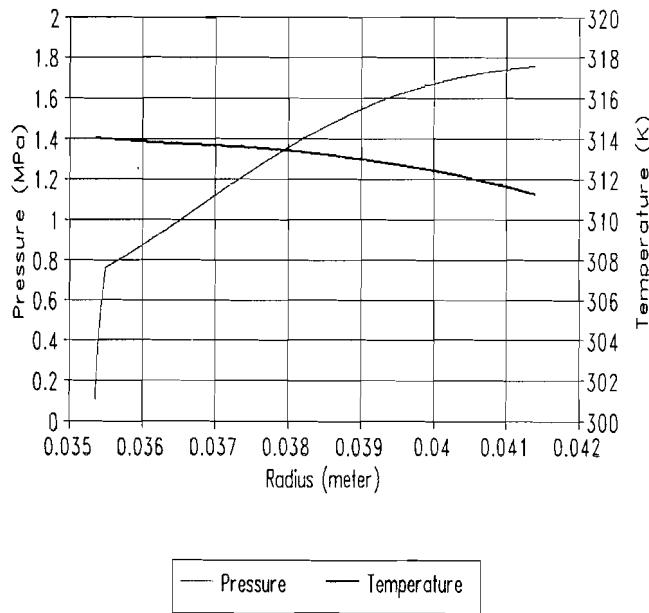


Fig. 13—Pressure and temperature distributions, two-phase seal.

caused by viscous shearing, is significantly higher than the gas seal. Increasing the heat removal rate could drastically reduce the face temperature and thermal deformation in the liquid seal operation. The above also suggests that there is a greater degree of uncertainty in the performance prediction for the liquid seal than for the gas seal.

### Two-Phase Seal

The two-phase seal in this analysis has the same configuration as the gas (propane) seal discussed previously. Although propane is in its liquid state in the pressurized chamber, it vaporizes when it leaks through the seal face due to the pressure drop. Therefore, liquid and vapor propane could coexist in the film. A typical pressure and temperature distribution of such a two-phase seal is shown in Fig. 13. The temperature is almost uniform across the seal face. The tem-

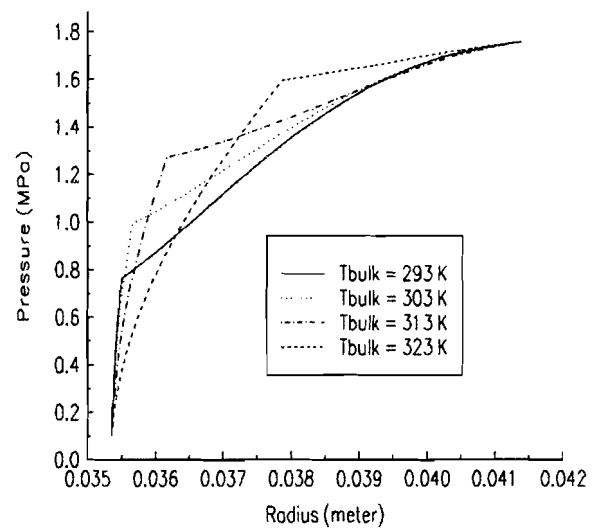


Fig. 14—Temperature effect on pressure distribution, two-phase seal.

perature difference between ID and OD is less than 3°K compared to the average bulk temperature (293°K). The pressure profile exhibits two different regions. The smaller region near the ID, where the pressure gradient is extremely high, is the vapor region, while the much larger region near the OD, where pressure change is moderate, is the liquid region. The location where the pressure slope is discontinuous is the phase change point. In this case, the phase change occurs very close to the ID. These results are similar to those of the water two-phase seal analyzed by Lebeck (24).

Figure 14 shows how the pressure distributions change with bulk fluid temperature. A total of four temperature points ranging from 293°K to 323°K were studied. When the bulk temperature is outside this range, no two-phase solution can be found: a lower temperature will not cause any vaporization and would yield an all liquid seal; a higher temperature causes propane to vaporize over the entire seal face, leading to an all gas seal. The boiling location moves toward the OD as temperature increases; therefore, the bulk fluid temperature has a strong impact on the phase change location and pressure distribution.

Figure 15 shows the film thickness distribution at various bulk temperatures. The average film thickness does not change much with bulk temperature, and the spatial variations are less than 0.3 microns.

From Fig. 16, it is seen that the leakage rate decreases as the temperature increases. When  $T_{bulk} = 323^{\circ}\text{K}$ , the vapor region is so extensive that the leakage rate is hardly different from the result of the same propane gas seal studied previously. This suggests that the two-phase seal behaves like a gas seal at high enough bulk temperatures, where most of the film is vaporized.

### CONCLUSIONS

Mechanical seal operation under mixed lubrication conditions is a complex process. It involves many coupled physical mechanisms, including film lubrication, asperity contact, thermal and mechanical deformations, possibly phase change, and viscosity-temperature dependency. In this study, a seal model that integrates these features has been established. An efficient computer code has been developed that can analyze the per-

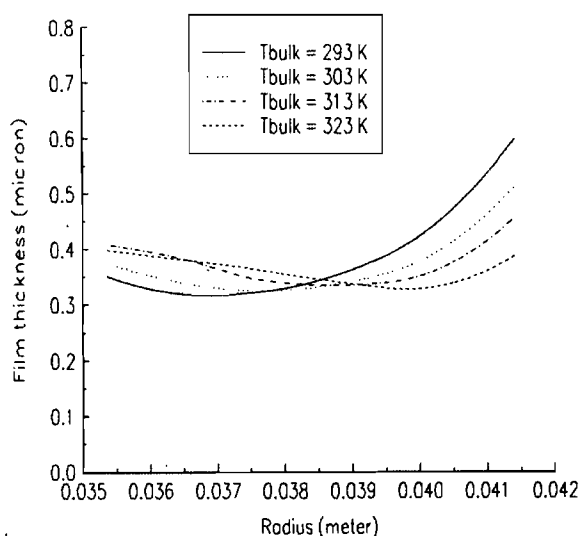


Fig. 15—Film thickness distribution, two-phase seal.

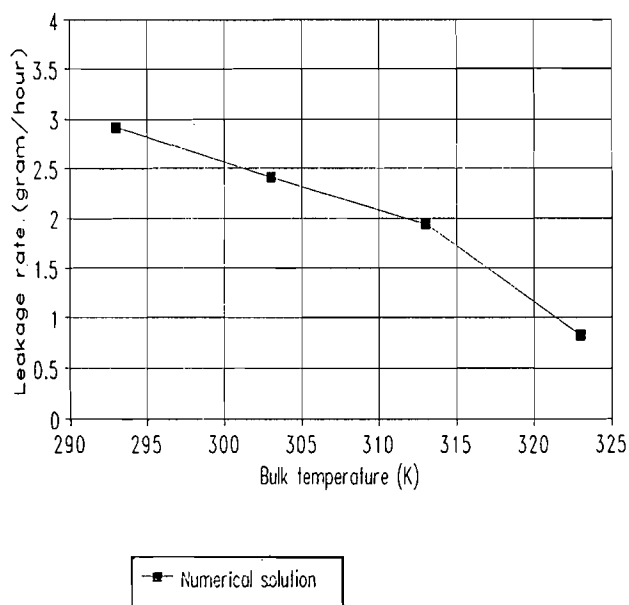


Fig. 16—Leakage rate, two-phase seal.

formance of seals under various operating conditions. Numerical solutions have been compared with available test data and good agreement has been found. Simulations based on the influence coefficient method have shown that accurate results can be obtained with this method. Thus, accuracy and efficiency can be achieved simultaneously. Use of the influence coefficient method results in central processing unit (cpu) times that are a fraction of those required if a finite element analysis was included in the iteration loop.

Based on the numerical simulation, it is seen the roughness orientation has an impact on the seal leakage. The asperity friction is the major source of heating in the gas seals while the viscous shearing dominates in the liquid seals. Thermal effects are more pronounced in liquid seals and two-phase

seals than in gas seals. In liquid seals, the face temperature could have considerable variation and is strongly dependent on the convective heat transfer process in the seal chamber. The uncertainty in the convective heat transfer coefficients and thermal boundary conditions significantly affect the prediction of the face temperature distribution, thermal deformation and, ultimately, the overall seal performance.

## REFERENCES

- (1) Tzeng, S. T. and Saibel, E., "Surface Roughness Effect on Slider Bearing Lubrication," *ASLE Trans.*, **10**, pp 334–338, (1967).
- (2) Christensen, H., "Stochastic Models for Hydrodynamic Lubrication of Rough Surfaces," in *Proc. IMechE*, **184**, pp 1013–1022, (1969).
- (3) Christensen, H. and Tønder, K., "Tribology of Rough Surfaces, A Stochastic Model of Mixed Lubrication," SINTEF (Stiftelsen for Industriell og Teknisk Forskning), Trondheim, Norway, SINTEF Report No. **18/70-21**, (1970).
- (4) Christensen, H. and Tønder, K., "The Hydrodynamic Lubrication of Rough Bearing Surfaces of Finite Width," *ASME Jour. of Lubr. Tech.*, **93**, pp 324–330, (1971).
- (5) Patir, N. and Cheng, H. S., "An Average Flow Model for Determining Effects of Three-Dimensional Roughness on Partial Hydrodynamic Lubrication," *ASME Jour. of Lubr. Tech.*, **100**, pp 12–17, (1978).
- (6) Patir, N. and Cheng, H. S., "Application of Average Flow Model to Lubrication Between Rough Sliding Surfaces," *ASME Jour. of Lubr. Tech.*, **101**, pp 220–230, (1979).
- (7) Elrod, H. G., "A General Theory for Laminar Lubrication with Reynolds Roughness," *ASME Jour. of Lubr. Tech.*, **101**, pp 8–14, (1979).
- (8) Tripp, J. H., "Surface Roughness Effects in Hydrodynamic Lubrication: The Flow Factor Method," *ASME Jour. of Lubr. Tech.*, **105**, pp 458–465, (1983).
- (9) Tønder, K., "Simulation of the Lubrication of Isotropically Roughness Surfaces," *ASLE Trans.*, **23**, 3, pp 326–333, (1979).
- (10) Teale, J. L. and Lebeck, A. O., "An Evaluation of the Average Flow Model for Surface Roughness Effects in Lubrication," *ASME Jour. of Lubr. Tech.*, **102**, pp 360–367, (1980).
- (11) Hu, Y. Z. and Zheng, L. Q., "Some Aspects of Determining the Flow Factors," *ASME Jour. of Trib.*, **111**, pp 525–531, (1986).
- (12) Abbott, E. J. and Firestone, F. A., "Specifying Surface Quality: A Method Based on Accurate Measurement and Comparison," *Mech. Eng.*, **55**, pp 569–572, (1933).
- (13) Pullen, J. and Williamson, J. B. P., "On the Plastic Contact of Rough Surfaces," in *Proc. of Roy. Soc. London*, **A 327**, pp 159–173, (1972).
- (14) Greenwood, J. A. and Williamson, J. B. P., "Contact of Nominally Flat Surfaces," in *Proc. of Roy. Soc. London*, **A 295**, pp 300–319, (1966).
- (15) Greenwood, J. A. and Tripp, J. H., "The Elastic Contact of Rough Spheres," *ASME Jour. of Appl. Mech.*, **34**, pp 153–159, (1967).
- (16) Chang, W. R., Etsion, I. and Bogy, D. B., "An Elastic-Plastic Model for the Contact of Roughness Surface," *ASME Jour. of Trib.*, **109**, pp 257–263, (1987).
- (17) Lebeck, A. O., "A Mixed Friction Hydrostatic Mechanical Face Seal Model with Thermal Rotation and Wear," *ASLE Trans.*, **23**, 4, pp 375–387, (1979).
- (18) Lebeck, A. O., "A Mixed Friction Hydrostatic Face Seal Model with Phase Change," *ASME Jour. of Lubr. Tech.*, **102**, pp 133–138, (1980).
- (19) Zhu, D., Cheng, H. S., Arai, T. and Hamai, K., "A Numerical Analysis for Piston Skirts in Mixed Lubrication—Part I: Basic Modeling," *ASME Jour. of Trib.*, **114**, pp 553–562, (1992).
- (20) Zhu, D., Hu, Y. Z., Cheng, H. S., Arai, T. and Hamai, K., "A Numerical Analysis for Piston Skirts in Mixed Lubrication—Part II: Deformation Consideration," *ASME Jour. of Trib.*, **115**, pp 125–133, (1993).
- (21) Yamaguchi, A. and Matsuoka, H., "A Mixed Lubrication Model Applicable to Bearing/Seal Parts of Hydraulic Equipment," *ASME Jour. of Trib.*, **114**, pp 116–121, (1992).
- (22) Etsion, I. and Front, I., "A Model for Static Sealing Performance of End Face Seals," *Trib. Trans.*, **37**, pp 111–119, (1994).
- (23) Ruan, B., "A Mixed Lubrication Model of Liquid/Gas Mechanical Seals," Ph.D. Dissertation, Georgia Institute of Technology, Atlanta, GA. (1995).
- (24) Lebeck, A. O., *Principles and Design of Mechanical Face Seals*, John Wiley & Sons, Inc., New York, (1991).